Optical Injection and Terahertz Detection of the Macroscopic Berry Curvature

Kuljit S. Virk*
Department of Chemistry, Columbia University, 3000 Broadway, New York, New York 10027, USA

J. E. Sipe†
Department of Physics and Institute for Optical Sciences, University of Toronto, 60 St. George Street, Toronto, Ontario, Canada, M5S 1A7

(Received 20 April 2011; published 14 September 2011)

We propose an experimental scheme to probe the Berry curvature of solids. Our method is sensitive to arbitrary regions of the Brillouin zone and employs only basic optical and terahertz techniques to yield a background-free signal. Using semiconductor quantum wells as a prototypical system, we discuss how to inject Berry curvature macroscopically and probe it in a way that provides information about the underlying microscopic Berry curvature.

DOI: 10.1103/PhysRevLett.107.120403 PACS numbers: 03.65.Vf, 72.25.−b, 73.21.Fg, 73.63.Hs

Berry's phase permeates many fields of physics. In quantum mechanics, the net phase acquired by a wave function during a cyclic change in the parameters of a Hamiltonian is a gauge-invariant quantity that has measurable effects. This quantity can be directly expressed in terms of a physical property, called the Berry curvature (BC), which relates to the Berry phase in much the same way as the gauge-invariant magnetic field relates to a gauge-dependent vector potential [1]. In materials science, it is rapidly becoming clear that the role of the BC is as fundamental as that of an energy band [2]. The representation of a position operator in terms of the Bloch states of a crystal is intimately related to the BC, and it thus appeared in the works of Adams and Blount [3] on the topic much earlier than the rigorous formulation by Berry [4]. In the 1990s, King-Smith and Vanderbilt introduced a theory of electric polarization of solids as a bulk quantity [5], the present version of which is grounded in Berry's phase [2,6]. In parallel to this, the BC has appeared as a central physical quantity in the work on the anomalous Hall effect in ferromagnetic materials [7,8] and the intrinsic mechanism of the spin Hall effect [9,10]. Haldane expressed the nonquantized part of the intrinsic Hall conductivity in terms of integral of the Berry connection (vector potential of BC) on the Fermi surface [11], thus recapturing the essence of Landau's Fermi liquid theory. Recent works also show the role of BC in the photogalvanic effect [12,13].

Central to these effects is anomalous velocity, which refers to motion of charges perpendicular to their usual group velocity [3]. As an average of the BC, it appears as its main experimental manifestation. Though the above works elucidate the role of the BC in explaining various phenomena, they are severely restricted as methods to probe it as a basic property of solids. This is because the dc response reduces to an integral of Berry curvature over the full Brillouin zone and, for a partially filled band, to the volume occupied by the carrier distribution function [11]. The measured response is thus restricted to either the full Brillouin zone or a slightly displaced equilibrium occupation function of a partially filled band.

This Letter presents a method to study this important and complementary quantity of solids, which is much less restricted in its sampling of the Brillouin zone. It was anticipated by the work of Moore and Orenstein [14], who showed how confinement in quantum wells induces a Berry's phase that leads to a helicity-dependent photocurrent. While we focus on the hole bands of a GaAs quantum well (see Fig. 1), chosen because of their large BC [9] with a rich structure, our method is very general and in principle can be applied to a wide range of materials. An optical excitation by circularly polarized light induces a nonzero transient macroscopic Berry curvature (TMBC) in such materials, due to the creation of a state that breaks time-reversal and space inversion symmetry. The injection is followed by a linearly polarized terahertz wave, which drives the optically injected carriers. In the presence of TMBC, the motion of charges has an anomalous component, which is perpendicular to the polarization of the terahertz (THz) wave. The detection of the radiated THz

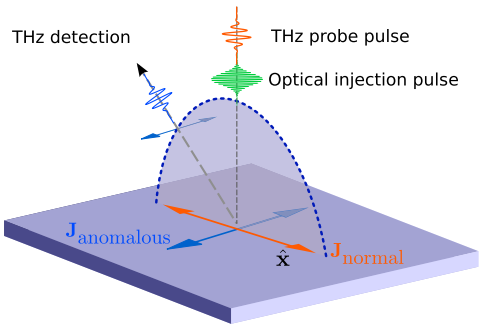

FIG. 1 (color online). Illustration of the proposed scheme for injection and detection of macroscopic Berry curvature.

field in the cross-polarized direction is thus entirely a signal due to the TMBC. Such a TMBC can be injected even in materials of Chern class zero, where an equilibrium MBC is not allowed [15]. This is in contrast to spin Hall insulators in which a net MBC exists in the ground state.

Our Letter is organized as follows. We begin with a discussion of the microscopic Berry curvature. We then discuss the optical injection of TMBC, its detection by linearly polarized THz excitation, and its intrinsic lifetime due to electron-hole scattering. Finally, we present the results of our numerical calculations of the microscopic and optically injected TMBC, followed by the results of the anomalous velocity induced by the THz excitation.

Microscopic Berry curvature: Bulk crystals.—The band theory of solids describes single electron wave functions by Bloch functions, $\psi_n(\boldsymbol{k};\boldsymbol{r})$, for energy bands $\varepsilon_n(\boldsymbol{k})$. Here n labels a single energy band with a continuous slope, starting from the energy levels at the center of the Brillouin zone [16]. Between two degenerate bands, or within a single band, the vector

$$\boldsymbol{\zeta}_{nm}(\boldsymbol{k}) = i\int d\boldsymbol{r} u_n^*(\boldsymbol{k};\boldsymbol{r})\frac{\partial}{\partial \boldsymbol{k}} u_m(\boldsymbol{k};\boldsymbol{r}) \tag{1}$$

acts like a vector potential in the momentum space dynamics of electrons, its dependence on the choice of the phases of the $\{u_m(\boldsymbol{k};\boldsymbol{r})\}$ leading to the analogue of a gauge dependence. Taking the curl of $\boldsymbol{\zeta}_{nm}(\boldsymbol{k})$ leads to the (microscopic) BC, a "gauge-invariant" quantity at each $\mathbf{k}$,

$$\Omega_{nm}^{\alpha}(\boldsymbol{k}) = [\nabla\times\zeta_{nm}(\boldsymbol{k})]^{\alpha} - i\epsilon_{\alpha\beta\gamma}\sum_{\varepsilon_p=\varepsilon_n=\varepsilon_m}[\zeta_{np}^{\beta}(\boldsymbol{k}),\zeta_{pm}^{\gamma}(\boldsymbol{k})]. \tag{2}$$

In the presence of time-reversal and spatial inversion symmetries, $\boldsymbol{\Omega}(\boldsymbol{k})$ takes the form of a traceless matrix within each degenerate subspace [3]; the MBC

$$\langle\boldsymbol{\Omega}\rangle \equiv \sum_{nm\boldsymbol{k}}\boldsymbol{\Omega}_{nm}(\boldsymbol{k})\rho_{mn}(\boldsymbol{k}),$$

where $\rho_{nm}(\boldsymbol{k})$ is the single particle density matrix, then vanishes in equilibrium; even in a material such as GaAs, where there is no inversion symmetry, the equilibrium MBC vanishes because the band structure is of Chern class zero. Away from equilibrium, such as in the dc response of a p-doped semiconductor, the MBC can play a role [8–10], but optically excited distributions allow much greater access to its local probing in $\mathbf{k}$ space.

Quantum wells.—We focus on the valence states of a quantum well, described by the Luttinger model of a square quantum well grown along the $[001]\equiv\hat{\mathbf{z}}$ direction. In this model [17] there are degenerate ($\pm$) wave functions described by 4-component spinors, labeled $\boldsymbol{f}_n^{\pm}(\mathbf{k};z)$ for each two-dimensional subspace n, and the microscopic BC is equal to $\hat{\mathbf{z}}\Omega_{nn}^{z}(\boldsymbol{k})\sigma^3$, where

$$\Omega_{nn}^{z}(\boldsymbol{k}) = \epsilon_{z\mu\nu}\int dz\,\partial_\mu \boldsymbol{f}_n^{-\dagger}(\boldsymbol{k};z)\cdot\partial_\nu \boldsymbol{f}_n^{-}(\boldsymbol{k};z), \tag{3}$$

and σ^3 is the third Pauli matrix. Figure 2 shows the top two valence energy bands and the corresponding Berry curvature for a 15 nm thick quantum well. The middle panel shows $\Omega_{nn}^{z}(k)$ defined in (3); large $\Omega_{nn}^{z}(k)$ results from a large mixing of two or more states [18], here arising because of contributions from the light hole to the two bands.

Macroscopic Berry curvature.—No macroscopic effect results from $\Omega_{nn}^{z}(\boldsymbol{k})$ unless an imbalance is created between the hole populations of the $\boldsymbol{f}^{\pm}$ states of these subspaces, leading to a nonzero $\langle\Omega^z\rangle$. In optical excitation across the band gap with left-circularly polarized light, the matrix elements connect $\boldsymbol{f}^{-}$ to the spin up conduction subbands with a probability $1/3$ of the corresponding transition from $\boldsymbol{f}_n^{+}$ to the same conduction subband. This yields a 3:1 population imbalance between the two otherwise degenerate states, leading to a nonvanishing $\langle\Omega^z\rangle$. The possibility of creating this imbalance in the nonequilibrium state is a well-established experimental fact [19]. A correction arises from the electron-hole interaction such that the final state is an exciton. This correction is small for ionization states (the only states relevant above the optical gap) and decreases the higher up we move in the band.

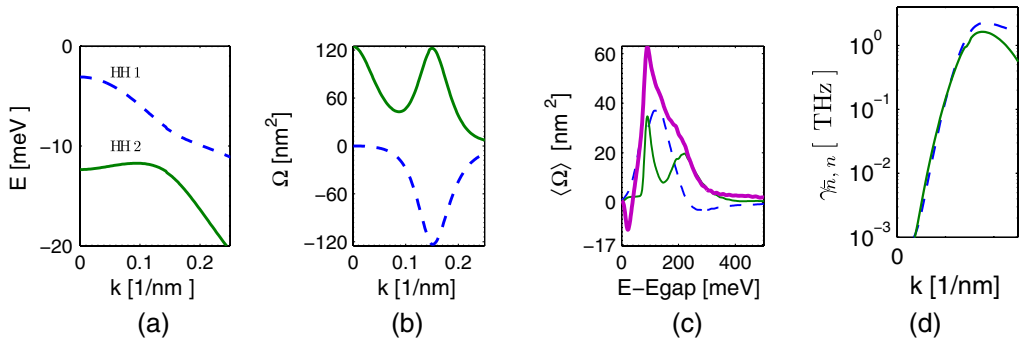

FIG. 2 (color online). (a) Highest valence (heavy) hole bands for a 15 nm thick [001] GaAs quantum well; (b) Berry curvature $\Omega^z(k)$ [lines as in (a)]; (c) $\langle\Omega^z\rangle$ (thick solid line) and $\langle\Omega_n^z\rangle$ for odd parity states [lines as in (a)]; (d) Coulomb scattering rate between the + and − states for optical excitation at 90 meV above gap energy. Lines as in (a).

To access $\langle\Omega^z\rangle$ we imagine a linearly polarized THz electric field $E(t)\hat{\mathbf{x}}$ driving the optically injected hole population. Terahertz excitation does not couple $\boldsymbol{f}_n^+$ and $\boldsymbol{f}_n^-$ states since there is no momentum matrix element between them, and therefore it does not disturb the injected $\langle\Omega^z\rangle$. The Schrödinger equation for the hole density matrix $\rho(\mathbf{k}, t)$ coupled to the external THz field polarized along $\hat{\mathbf{x}}$ (or [100]) direction reads

$$i\left(\hbar\frac{\partial}{\partial t} + eE^x(t)\frac{\partial}{\partial k_x}\right)\rho(\boldsymbol{k}, t) = [H_0(\boldsymbol{k}) + eE^x(t)\zeta^x(\boldsymbol{k}), \rho(\boldsymbol{k}, t)] + \dot{\rho}|_{\text{scatt}}. \quad (4)$$

Here $H_0(\boldsymbol{k})$ is the Luttinger Hamiltonian, and the last term is the contribution of Coulomb scattering. A gauge transformation exists such that $\zeta^x(\boldsymbol{k}) = 0$ locally in the region of interest, and within this gauge we can easily compute the solution of (4) with $\rho(\boldsymbol{k}, 0)$ set equal to the hole populations created by optical excitation. The expectation value of the velocity operator $\mathbf{v}$ is then calculated at each time point to study the macroscopic motion of charges:

$$\langle\boldsymbol{v}(t)\rangle = \sum_{\boldsymbol{k}}\rho_{nm}(\boldsymbol{k}, t)\mathbf{v}_{mn}(\boldsymbol{k}). \quad (5)$$

Sum rules that relate $\boldsymbol{\Omega}$ to $\boldsymbol{\zeta}$ [16] can be used to show that in the linear regime an anomalous contribution to the average velocity may exist and is proportional to the macroscopic Berry curvature:

$$\langle\boldsymbol{v}(t)\rangle_{\text{anomalous}} = -\hat{\mathbf{y}}\frac{e}{\hbar}\langle\Omega^z\rangle E^x(t), \quad (6)$$

until $\langle\Omega^z\rangle$ decays due to scattering between the $\pm$ state populations, primarily through the dynamic polarizability of the electron gas, described by the term $\dot{\rho}|_{\text{scatt}}$. The electrons generated by the optical excitation would always diminish the Berry phase effects, and therefore this is an intrinsic lifetime because it survives in the limit of no impurities. The self-energy effects may be decomposed into two contributions: (A) decoherence within each set (either + or −) of states and (B) population transfer between the sets of states. Type A limits the sensitivity of the dynamics within each set to the microscopic BC, while type B reduces the net effect of MBC; B effects degrade the signal more effectively than A effects by restoring the time-reversal symmetry broken by the initial optical excitation.

We model these effects by setting $\dot{\rho}_{nm}(\boldsymbol{k}, t)|_{\text{scatt}} = -\eta_{nm}\rho_{nm}(t)$ for off-diagonal terms (type A; n and m in the same set) and $\dot{\rho}_{nn}(\boldsymbol{k}, t)|_{\text{scatt}} = -\gamma_{n\bar{n}}(\boldsymbol{k})[\rho_{nn}(\boldsymbol{k}, t) - \rho_{\bar{n}\bar{n}}(\boldsymbol{k}, t)]$ for population relaxation terms [type B; here $n(\bar{n})$ refers to the $\boldsymbol{f}_n^+$ ($\boldsymbol{f}_n^-$) state]. To estimate the rates $\gamma_{nm}(\boldsymbol{k})$ and $\gamma_{n\bar{n}}(\boldsymbol{k})$, we start with the RPA self-energy, employ the generalized Kadanoff-Baym ansatz [20], and follow by the Markov approximation. The Auger scattering of holes by electrons is negligible, due to the energy conservation condition at each vertex in the self-energy diagram.

Results and discussion.—For excitation with a 100 fs Gaussian optical pulse, the resulting $\langle\Omega^z\rangle$ is shown as a function of energy above the band gap in the third panel of Fig. 2. The panel also shows the breakdown of $\langle\Omega^z\rangle$ into contributions from the individual bands. The initial rise in $\langle\Omega^z\rangle$ is entirely due the first band, in which the dominance of $\boldsymbol{f}^+$ component leads to the sign opposite to its microscopic counterpart in the middle panel. The large contribution from the second band starts to dominate above 85 meV.

The rightmost panel in Fig. 2 shows the scattering rate $\gamma_{n,\bar{n}}(k)$ for each of the two bands at a carrier density of 10^{11} cm^{-2}. The rate remains below 1 THz and is suppressed at small k, where the spinors have orthogonal dominant contributions. We find that the $\eta_{nm}(k)$ range between 1 and 4 THz, but their effect on the THz dynamics is only secondary as discussed in relation to type A interactions. So we can expect that $\langle\Omega^z\rangle$ does not vanish during the subsequent THz probe. Thus we see that the effects of relevant scattering between electrons and holes are significantly suppressed by symmetries of the well.

We now turn to the results of our numerical solution of (4) and present the normal and anomalous hole velocities calculated via (5). The field is polarized along $\hat{\mathbf{x}}$ so that the anomalous velocity is along $\hat{\mathbf{y}}$; see Fig. 1. Our calculations are performed with $E(t) = E_0 e^{-(t-t_0)^2/2\tau_p^2}\cos(\omega_0 t)$. We chose $E_0 = 0.1$ kV/cm, $\omega_0 = 1$ THz, $\tau_p = 1$ ps, and t_0 a conveniently chosen point in time. By comparing the velocities with and without the $\dot{\rho}|_{\text{scatt}}$ term in (4), we found that the anomalous velocity is reduced by $\simeq 36\%$, while the normal velocity undergoes little change by scattering as expected.

In Fig. 3, we demonstrate the relationship between the magnitude of $\langle v_y(t)\rangle$, $\langle\Omega^z\rangle$, and the hole populations for different photon energies above the gap; large anomalous velocities clearly arise when the Berry curvature of the populated states is large. These calculations lie in the linear regime, where (6) is a good approximation; in the nonlinear regime, no clearcut relationship exists between the expectation value of the velocity operator and the $\langle\Omega^z\rangle$ as the concept of intraband motion itself breaks down.

As shown in Fig. 1, the anomalous velocity could be detected by measuring the emitted THz radiation polarized perpendicular to the incident field. While the much lighter electrons in the conduction band would also emit THz radiation, and at much higher power than the holes, the Berry curvature of conduction bands in these quantum wells vanishes. So only the anomalous velocity of holes would contribute to the THz emission perpendicular to the incident field. In addition, by placing the THz detector at an oblique angle in the plane of the incident field vector, the dipole field of the parallel component can be highly suppressed while leaving the perpendicular component

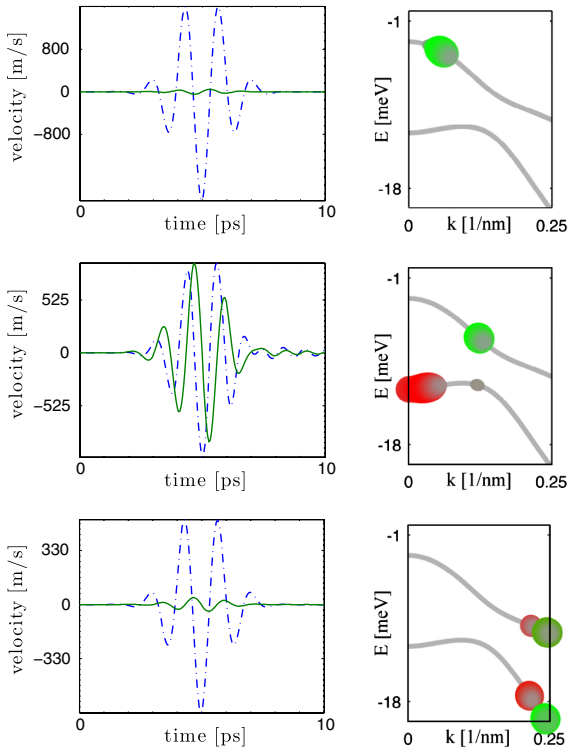

FIG. 3 (color online). THz induced velocities (left) and populations (right) at 20, 90, and 350 meV (top to bottom) for a 15 nm wide quantum well. Anomalous (normal) velocities are in solid (dashed-dotted) lines.

unaffected. Separation of the desired signal from background is thus already built into this method.

In the above analysis, we took only intrinsic scattering due to Coulomb interaction among electrons into account. We emphasize that a large hole mobility is crucial to the experimental success of this scheme. Spin-flip scattering of holes is an approximate concept in this scenario, but it is a useful characterization of the detrimental effects of impurity scatterers in our scheme. It is suppressed exponentially close to the Γ point but rises sharply to rates faster than 1 THz as a function of k for areal concentrations of 10^{10} cm^{-2} [21]. The effects of phonons are subtle. On the one hand, they may provide a dominant scattering channel. On the other hand, as observed previously, only those scattering events that link the partner states are actually detrimental. Detailed calculations of these effects, including lattice vibrations, are the focus of our ongoing work.

In conclusion, we have shown that significant macroscopic Berry curvature can be injected in GaAs quantum wells by circularly polarized light. The lifetime of this macroscopic effect is at least a few picoseconds, and its robustness results from the properties of hole wave functions under the symmetry operations of the quantum well. We have presented a scheme to make this macroscopic effect accessible experimentally via the anomalous contribution to the THz emission from a quantum well driven by a linearly polarized THz field. A successful implementation of this scheme would open up a new venue in exploration of the Berry curvature as a fundamental property of solids.

The authors acknowledge financial support from Natural Sciences and Research Council of Canada. We thank Ali Najmaie and Sangam Chatterjee for insightful discussions.

*kv2212@columbia.edu
†sipe@physics.utoronto.ca

[1] *Geometric Phases in Physics*, edited by F. Wilczek and A. Shapere (World Scientific, Singapore, 1989), Vol. 5.
[2] R. M. Martin, *Electronic Structure: Basic Theory and Practical Methods* (Cambridge University Press, Cambridge, England, 2003).
[3] E. I. Blount, in *Advances in Research and Applications*, edited by F. Seitz and D. Turnbull, Solid State Physics Vol. 13 (Academic, New York, 1962), pp. 305–373.
[4] M. V. Berry, Proc. R. Soc. A **392**, 45 (1984).
[5] D. Vanderbilt and R. D. King-Smith, Phys. Rev. B **48**, 4442 (1993).
[6] R. Resta, Rev. Mod. Phys. **66**, 899 (1994).
[7] S. Onoda, N. Sugimoto, and N. Nagaosa, Phys. Rev. B **77**, 165103 (2008).
[8] T. Jungwirth, Q. Niu, and A. H. MacDonald, Phys. Rev. Lett. **88**, 207208 (2002).
[9] S. Murakami, Adv. Solid State Phys. **45**, 197 (2006).
[10] H.-a. Engel, E. I. Rashba, and B. I. Halperin, in *Handbook of Magnetism and Advanced Magnetic Materials*, edited by H. Kronmüller and S. Parkin (Wiley, Chichester, 2007), pp. 2858–2877.
[11] F. D. M. Haldane, Phys. Rev. Lett. **93**, 206602 (2004).
[12] E. Deyo, L. Golub, E. Ivchenko, and B. Spivak, arXiv:0904.1917.
[13] P. Hosur, Phys. Rev. B **83**, 035309 (2011).
[14] J. E. Moore and J. Orenstein, Phys. Rev. Lett. **105**, 026805 (2010).
[15] M. Hasan and C. Kane, Rev. Mod. Phys. **82**, 3045 (2010).
[16] M. Lax, *Symmetry Principles in Solid State and Molecular Physics* (Dover, Mineola, MN, 2001).
[17] L. C. Andreani, A. Pasquarello, and F. Bassani, Phys. Rev. B **36**, 5887 (1987).
[18] To verify, use $\boldsymbol{k} \cdot \boldsymbol{p}$ expansion and (1) and (2).
[19] A. Najmaie, R. D. R. Bhat, and J. E. Sipe, Phys. Rev. B **68**, 165348 (2003).
[20] P. Lipavsky, V. Špička, and B. Velicky, Phys. Rev. B **34**, 6933 (1986).
[21] R. Ferreira and G. Bastard, Phys. Rev. B **43**, 9687 (1991).